Memorias del XX Congreso Latinoamericano de Control Automático (CLCA 2025)
13-17 de Octubre, 2025. Cancún, Quintana Roo, México

On the observability of different output configurations for quadrotor UAVs

Alejandro Gutierrez-Giles * **Suping Zhao** **
Alejandra de la Guerra ***

* *Instituto Nacional de Astrofísica, Óptica y Electrónica, Luis Enrique Erro 1, San Andrés Cholula, Puebla, México (e-mail:alejandro.giles@inaoe.mx)*
** *Xi'an Technological University. No. 2 Xuefuzhonglu Road, Weiyang District, Xi'an City, Shaanxi Province, China (e-mail:zhaosuping@xatu.edu.cn)*
*** *Universidad de las Américas Puebla, Ex-Hacienda Santa Catarina Mártir, 72810, San Andrés Cholula, Puebla, México (e-mail:alejandra.delaguerra@udlap.mx)*

Abstract: An observability analysis of a dynamical model of a quadrotor UAV is presented for four different sensor configurations of interest. The dynamic model is obtained by employing the Euler–Lagrange formulation. Then the observability analysis is carried out by employing nonlinear geometrical tools. The results obtained show some non intuitive results such as nonuniformly observability for some cases. A simulation study is also presented to validate the analysis.

Keywords: Observers, fault detection, unmanned autonomous vehicles.

1. INTRODUCTION

Recently, Unmanned Aerial Vehicles (UAV) have been extensively studied thanks to their many applications that range from infrastructure inspection (Parlange et al., 2018), surveillance (Ramachandran and Sangaiah, 2021), natural disasters response (Quero and Martinez-Carranza, 2025), aerial photography (Wang et al., 2023), crop monitoring Olivares-Figueroa et al. (2024), and even delivery services Vazquez-Meza and Martinez-Carranza (2024), among others.

For implementing an automatic controller, it is necessary to obtain feedback of the UAV position, orientation, and linear and angular velocities. Most UAVs are equipped with an inertial measurement unit (IMU). The IMU includes an accelerometer, a gyroscope, and, in some cases, a magnetometer. With the accelerometer and the gyroscope, the IMU can sense linear acceleration and angular rate. In turn, the magnetometer works as the UAV's compass.

To obtain information about the drone position with respect to an object or a fixed frame, most UAVs rely on external sensors, such as global positioning systems (GPS) or motion capture systems. Nevertheless, these systems have some drawbacks, e.g. the low accuracy of the GPS, and its lack of reliability on noncovered zones, and the low portability of the motion capture systems, leaving out the high costs of both systems. An attractive alternative consists in employing low-cost video cameras and some algorithm such as the so-called Simultaneous Localization and Mapping (SLAM). Although these algorithms are nowadays a standard in several robotic systems (Sonugür, 2023), there are still not sufficient for its use in feedback for advanced control techniques due to their low latency and its high computational cost.

In summary, there is a great amount of active research on signals estimation for UAVs not only for high-performance control applications, but for fault-detection, fault-tolerant controllers, system monitoring, and so on.

In this work, we aim to theoretically analyze the observability properties of some combinations of state measurements, which can be of interest in several applications. Four cases are presented and analyzed by employing geometrical tools, leading to non intuitive conclusions in some of the cases.

The paper is organized as follows: in Section 2, the UAV kinematic and dynamic models employed for the analysis are introduced. In Section 3 the observability analysis is presented. A discussion about the results of the analysis is presented in Section 4. Finally, some concluding remarks and directions for future work are given in Section 5.

https://doi.org/10.58571/CNCA.AMCA.2025.041

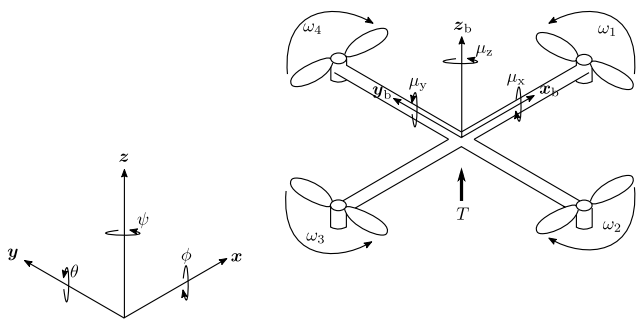

Fig. 1. Quadcopter with X configuration

2. MATHEMATICAL MODEL

In this section a mathematical model of the UAV is presented. An oversimplified representation of an UAV quadcopter (Luukkonen, 2011; Artale et al., 2013) is shown in Figure 1.

2.1 Kinematics

For obtaining a suitable mathematical model to carry out the different observability analysis, the Euler-Lagrange formulation is employed here. Let us start with the definition of the so-called generalized coordinates, defined by

$$\boldsymbol{\xi} = \begin{bmatrix} x \\ y \\ z \end{bmatrix}, \boldsymbol{\eta} = \begin{bmatrix} \phi \\ \theta \\ \psi \end{bmatrix}, \boldsymbol{q} = \begin{bmatrix} \boldsymbol{\xi} \\ \boldsymbol{\eta} \end{bmatrix}, \tag{1}$$

where $\boldsymbol{\xi} \in \mathbb{R}^{\not\vdash}$ is the position of the quadcopter frame origin with respect to a fixed frame, $\boldsymbol{\eta} \in \mathbb{R}^{\not\vdash}$ is the vector accounting for roll-pitch-yaw angles which represent the rotation of the UAV frame with respect to the fixed frame. These six coordinates are bounded in the vector $\boldsymbol{q}$, of generalized coordinates.

The rotation matrix of the body frame with respect to the fixed frame can be computed from the roll-pitch-yaw angles above, as

$$\boldsymbol{R}_{\mathrm{b}} = \begin{bmatrix} C_\psi C_\theta & C_\psi S_\theta S_\phi - S_\psi C_\theta & C_\psi S_\theta C_\phi - S_\psi S_\phi \\ S_\psi C_\theta & S_\psi S_\theta S_\phi - C_\psi C_\phi & S_\psi S_\theta C_\phi - C_\psi S_\phi \\ -S_\theta & C_\theta S_\phi & C_\theta C_\phi \end{bmatrix}. \tag{2}$$

The linear velocities in body frame coordinates are defined by the vector ${}^{\mathrm{b}}\boldsymbol{v}_B$ and the angular velocities, or angular rates, are defined by

$${}^{\mathrm{b}}\boldsymbol{v}_B = \begin{bmatrix} v_{x,B} \\ v_{y,B} \\ v_{z,B} \end{bmatrix}, {}^{\mathrm{b}}\boldsymbol{\omega} = \begin{bmatrix} \omega_{\mathrm{x}} \\ \omega_{\mathrm{y}} \\ \omega_{\mathrm{z}} \end{bmatrix}, \tag{3}$$

where $\boldsymbol{\omega} \in \mathcal{R}^3$ is the vector or angular velocities with respect to the body frame axes. The relation between the angular velocities in the body frame and the roll-pitch-yaw time derivatives in the fixed frame is given by

$${}^{\mathrm{b}}\boldsymbol{\omega} = \boldsymbol{W}_\eta \dot{\boldsymbol{\eta}}, \tag{4}$$

where

$$\boldsymbol{W}_\eta = \begin{bmatrix} 1 & 0 & -S_\theta \\ 0 & C_\phi & S_\phi C_\theta \\ 0 & -S_\phi & C_\phi C_\theta \end{bmatrix}, \tag{5}$$

with $S_x = \sin(x)$, $C_x = \cos(x)$ and $T_x = \tan(x)$.

2.2 Euler-Lagrange formulation

There are different ways to obtain a dynamic model for the quadcopter motion equations, such as the Newton-Euler formulation. In this work, we employ the well known Euler-Lagrange equations. The starting point for employing this method is to define the kinetic and potential energies in terms of the generalized coordinates. We define all the coordinates with respect to the fixed frame. First, the kinetic energy is defined by

$$\mathcal{K} = \frac{1}{2} \dot{\boldsymbol{q}}^{\mathrm{T}} \boldsymbol{H}(\boldsymbol{q}) \dot{\boldsymbol{q}}, \tag{6}$$

where the matrix $\boldsymbol{H}(\boldsymbol{q})$ is the inertia matrix defined as

$$\boldsymbol{H}(\boldsymbol{q}) = m \boldsymbol{J}_{\mathrm{v}}^{\mathrm{T}} \boldsymbol{J}_{\mathrm{v}} + \boldsymbol{J}_{\omega}^{\mathrm{T}} \boldsymbol{R}_{\mathrm{b}} \boldsymbol{I}_{\mathrm{b}} \boldsymbol{R}_{\mathrm{b}}^{\mathrm{T}} \boldsymbol{J}_{\omega}, \tag{7}$$

where $m \in \mathcal{R}$ is the drone mass, $\boldsymbol{I}_{\mathrm{b}} \in \mathcal{R}^{3\times3}$ is the drone inertia tensor in the body frame, which here is considered diagonal for simplicity, i.e. $\boldsymbol{I}_{\mathrm{b}} = \mathrm{diag}(I_{\mathrm{x}}, I_{\mathrm{y}}, I_{\mathrm{z}})$, and $\boldsymbol{J}_{\mathrm{v}} \in \mathcal{R}^{3\times6}$ and $\boldsymbol{J}_{\omega} \in \mathcal{R}^{3\times6}$ are the linear and angular velocities Jacobians, respectively, given by

$$\boldsymbol{J}_{\mathrm{v}} = [\boldsymbol{I}_3 \ \boldsymbol{O}_3] \tag{8}$$

$$\boldsymbol{J}_{\omega} = [\boldsymbol{O}_3 \ \boldsymbol{R}_{\mathrm{b}} \boldsymbol{W}_\eta], \tag{9}$$

where $\boldsymbol{I}_3$ is the 3×3-identity matrix and $\boldsymbol{O}_3$ is a 3×3-matrix filled with zeros.

Second, the potential energy is simply given by

$$\mathcal{P} = m \bar{\boldsymbol{g}}^{\mathrm{T}} \boldsymbol{\xi}, \tag{10}$$

where $\bar{\boldsymbol{g}} = [0 \ 0 \ g_0]$, with g_0 the gravity acceleration constant.

Then, the Lagrangian is defined as

$$\mathcal{L} = \mathcal{K} - \mathcal{P} \tag{11}$$

and the Euler-Lagrange equations are given by

$$\frac{\mathrm{d}}{\mathrm{d}t}\left(\frac{\partial \mathcal{L}}{\partial \dot{\boldsymbol{q}}}\right) - \frac{\partial \mathcal{L}}{\partial \boldsymbol{q}} = \boldsymbol{\tau} - \boldsymbol{\tau}_{\mathrm{f}}, \tag{12}$$

where $\boldsymbol{\tau} \in \mathcal{R}^6$ is the vector of the generalized forces according to the directions of the generalized coordinates, and $\boldsymbol{\tau}_{\mathrm{f}} \in \mathcal{R}^6$ is the vector of damping forces. The generalized forces vector is defined as $\boldsymbol{\tau} = [\boldsymbol{T} \ \boldsymbol{\mu}]^{\mathrm{T}}$, where $\boldsymbol{T} \in \mathcal{R}^3$ is the linear motion thrust and $\boldsymbol{\mu} \in \mathcal{R}^3$ is the vector of angular torques in fixed frame.

The damping forces term in generalized coordinates can be written as

$$\boldsymbol{\tau}_{\mathrm{f}}(\boldsymbol{q}, \dot{\boldsymbol{q}}) = \begin{bmatrix} \boldsymbol{D}_\xi \dot{\boldsymbol{\xi}} \\ \boldsymbol{D}_\omega \boldsymbol{W}_\eta(\boldsymbol{q}) \dot{\boldsymbol{\eta}} \end{bmatrix} = \boldsymbol{D}(\boldsymbol{q}) \dot{\boldsymbol{q}}, \tag{13}$$

where $\boldsymbol{D}_\xi \in \mathcal{R}^{3\times3}$ and $\boldsymbol{D}_\omega \in \mathcal{R}^{3\times3}$ are diagonal matrices of damping coefficients for linear and angular motions, respectively, and $\boldsymbol{D}(\boldsymbol{q}) = \text{block diag}\big(\boldsymbol{D}_\xi, \boldsymbol{D}_\omega \boldsymbol{W}_\eta(\boldsymbol{q})\big)$.

 https://doi.org/10.58571/CNCA.AMCA.2025.041

In turn, the gravity forces vector in fixed frame is simply computed by

$$\boldsymbol{G}(\boldsymbol{q}) = \frac{\partial \mathcal{L}}{\partial \boldsymbol{q}}\,. \tag{14}$$

Finally, the Lagrangian model of the quadrotor is given by

$$\boldsymbol{H}(\boldsymbol{q})\ddot{\boldsymbol{q}} + \boldsymbol{C}(\boldsymbol{q},\dot{\boldsymbol{q}})\dot{\boldsymbol{q}} + \boldsymbol{D}(\boldsymbol{q})\dot{\boldsymbol{q}} + \boldsymbol{G}(\boldsymbol{q}) = \boldsymbol{\tau}\,, \tag{15}$$

where $\boldsymbol{C}(\boldsymbol{q},\dot{\boldsymbol{q}}) \in \mathcal{R}^{6\times 6}$ is a matrix that can be computed by using the Christoffel symbols of the first kind (Spong et al., 2006).

3. OBSERVABILITY ANALYSIS

In this section, some sensor configurations of interest are analyzed to investigate if it is possible to reconstruct all the signals required for control, monitoring, fault detection, and other applications. The signals of interest are the states of the dynamic system, for which the following state vector is defined

$$\boldsymbol{x} = [\boldsymbol{q}\ \dot{\boldsymbol{q}}]^{\mathrm{T}} = \left[\boldsymbol{\xi}\ \boldsymbol{\eta}\ \dot{\boldsymbol{\xi}}\ \dot{\boldsymbol{\eta}}\right]^{\mathrm{T}}\,. \tag{16}$$

Thus, the state-space model can be put in the form

$$\dot{\boldsymbol{x}} = \boldsymbol{f}(\boldsymbol{x}) + \boldsymbol{g}(\boldsymbol{x})\boldsymbol{u} \tag{17}$$

$$\boldsymbol{y} = \boldsymbol{h}(\boldsymbol{x})\,, \tag{18}$$

where

$$\boldsymbol{f}(\boldsymbol{x}) = \begin{bmatrix} \dot{\boldsymbol{q}} \\ -\boldsymbol{H}^{-1}(\boldsymbol{q})\Big(\boldsymbol{C}(\boldsymbol{q},\dot{\boldsymbol{q}})\dot{\boldsymbol{q}} + \boldsymbol{D}(\boldsymbol{q})\dot{\boldsymbol{q}} + \boldsymbol{G}(\boldsymbol{q})\Big) \end{bmatrix} \tag{19}$$

$$\boldsymbol{g}(\boldsymbol{x}) = \boldsymbol{H}^{-1}(\boldsymbol{q}) \begin{bmatrix} \boldsymbol{R}_{\mathrm{b}} & \boldsymbol{O}_3 \\ \boldsymbol{O}_3 & \boldsymbol{W}_{\eta}^{\mathrm{T}} \end{bmatrix}\,, \tag{20}$$

$\boldsymbol{u} = \left[{}^{\mathrm{b}}\boldsymbol{T}\ {}^{\mathrm{b}}\boldsymbol{\mu}\right]^{\mathrm{T}}$ is the vector of inputs, and $\boldsymbol{y}$ is the vector of outputs (measured states).

There are several definitions of observability. Roughly speaking, a nonlinear system (17)–(18) is observable if the whole state $\boldsymbol{x}$ at time t can be reconstructed from the solely information of the inputs $\boldsymbol{u}$ and the outputs $\boldsymbol{y}$ of the system up to time t. The observability question can be also stated as: given the measured inputs $\boldsymbol{u}$ and outputs $\boldsymbol{y}$ from time t_0 to time t, it is possible to reconstruct the initial condition of the whole state $x(t_0)$? More formal definitions of observability can be found in Besançon (2007).

The following theorem, originally proposed in Hermann and Krener (1977) will be the base point of the analysis.

Theorem 3.1. (Isidori, 1985) Let

$$\dot{\boldsymbol{x}} = \boldsymbol{f}(\boldsymbol{x}) + \boldsymbol{g}(\boldsymbol{x})\boldsymbol{u}$$

$$\boldsymbol{y} = \boldsymbol{h}(\boldsymbol{x})\,,$$

where $\boldsymbol{x}$ is a manifold of dimension n. Let $\mathcal{O}$ be the set of all finite linear combinations formed with the Lie derivatives of $h_1, h2, h3, ...h_p$ with respect to the $\boldsymbol{f}(\boldsymbol{x})$ and $\boldsymbol{g}(\boldsymbol{x})$ vector fields. Let $\mathrm{d}\mathcal{O}$ denote the set of the gradients of the elements of $\mathcal{O}$. The system is weakly (locally) observable if the observability rank condition is satisfied at x_0, that is, $\mathrm{d}\mathcal{O}$ contains n linearly independent vectors. □

In this work, we present four cases of interest, which are motivated from practical applications for quadrotor control, namely

- Case 1: Linear positions and roll-pitch-yaw angles are measured, i.e. $\boldsymbol{y} = \left[\boldsymbol{\xi}^{\mathrm{T}}\ \boldsymbol{\eta}^{\mathrm{T}}\right]^{\mathrm{T}}$.
- Case 2: Only roll-pitch-yaw angles are measured, i.e. $\boldsymbol{y} = \boldsymbol{\eta}$.
- Case 3: Only Cartesian positions are measured, i.e. $\boldsymbol{y} = \boldsymbol{\xi}$.
- Case 4: All three Cartesian positions and the yaw (ψ) angle are measured, i.e. $\boldsymbol{y} = [x\ y\ z\ \psi]^{\mathrm{T}}$.

Since the analysis based on Theorem 3.1 is local, we consider that the operation condition of interest for all four cases is around *hoovering*, i.e. when the UAV is in a horizontal off-ground position given by $\boldsymbol{\xi}_0 = [x_0\ y_0\ z_0]^{\mathrm{T}}$, where (x_0, y_0, z_0) is an arbitrary Cartesian position with $z_0 \neq 0$, $\dot{\boldsymbol{\xi}}_0 = \boldsymbol{0}$, $\boldsymbol{\eta}_0 = \boldsymbol{0}$, $\dot{\boldsymbol{\eta}}_0 = \boldsymbol{0}$.

For the following analysis, since we have four inputs, i.e. $\boldsymbol{u}$ is of dimension 4, then we must separate the vector field $\boldsymbol{g}(\boldsymbol{x})\boldsymbol{u}$ into four vector fields as

$$\boldsymbol{g}(\boldsymbol{x})\boldsymbol{u} = \boldsymbol{g}_1(\boldsymbol{x})u_1 + \boldsymbol{g}_2(\boldsymbol{x})u_2 + \boldsymbol{g}_3(\boldsymbol{x})u_3 + \boldsymbol{g}_4(\boldsymbol{x})u_4\,, \tag{21}$$

where $u_1 = T$, $u_2 = \mu_\phi$, $u_3 = \mu_\theta$, and $u_4 = \mu_\psi$. In fact, it is easy to check that $\boldsymbol{g}_i(\boldsymbol{x}) = \boldsymbol{g}_i(\boldsymbol{\eta}), i = 1, \ldots, 4$, i.e. the vector fields $\boldsymbol{g}_i$ do not depend on the position $\boldsymbol{\xi}$.

3.1 Case 1

In this case we are considering $\boldsymbol{y} = \left[\boldsymbol{\xi}^{\mathrm{T}}\ \boldsymbol{\eta}^{\mathrm{T}}\right]^{\mathrm{T}}$. This is a well known case in the control of UAVs, since it is known that in this case it is possible to reconstruct both linear and angular velocities. Nevertheless we carry out the analysis to illustrate the method. To construct the observability space $\mathcal{O}$, let us start with the differential of the output, namely

$$\mathrm{d}\boldsymbol{h} = \frac{\partial \boldsymbol{h}}{\partial \boldsymbol{x}} = \begin{bmatrix} \boldsymbol{I}_3 & \boldsymbol{O}_3 & \boldsymbol{O}_3 & \boldsymbol{O}_3 \\ \boldsymbol{O}_3 & \boldsymbol{I}_3 & \boldsymbol{O}_3 & \boldsymbol{O}_3 \end{bmatrix}\,. \tag{22}$$

By computing the Lie derivative along $\boldsymbol{f}$ one obtains

$$L_f\boldsymbol{h} = \frac{\partial \boldsymbol{h}}{\partial \boldsymbol{x}}\boldsymbol{f} = \begin{bmatrix} \dot{\boldsymbol{\xi}} \\ \dot{\boldsymbol{\eta}} \end{bmatrix}\,, \tag{23}$$

Now, by computing the differential of this last vector field

$$\mathrm{d}L_f\boldsymbol{h} = \begin{bmatrix} \boldsymbol{O}_3 & \boldsymbol{O}_3 & \boldsymbol{I}_3 & \boldsymbol{O}_3 \\ \boldsymbol{O}_3 & \boldsymbol{O}_3 & \boldsymbol{O}_3 & \boldsymbol{I}_3 \end{bmatrix}\,. \tag{24}$$

By stacking together the two differentials, it is not difficult to see that the observability matrix

$$\mathcal{O} = \begin{bmatrix} \mathrm{d}\boldsymbol{h} \\ \mathrm{d}L_f\boldsymbol{h} \end{bmatrix} \tag{25}$$

is always full-rank, and therefore the system is observable when measured this output. Furthermore, the observability does not depend on the inputs.

 https://doi.org/10.58571/CNCA.AMCA.2025.041

3.2 Case 2

In this case, we assume that only roll-pitch-yaw angles are measured, for which $\boldsymbol{y} = \boldsymbol{\eta}$. For this case, the first differential is given by

$$\mathrm{d}\boldsymbol{h} = [\boldsymbol{O}_3 \ \boldsymbol{I}_3 \ \boldsymbol{O}_3 \ \boldsymbol{O}_3] \ . \tag{26}$$

Then, we compute the Lie derivative along $\boldsymbol{f}$

$$L_f\boldsymbol{h} = \dot{\boldsymbol{\eta}} \, , \tag{27}$$

whose differential is

$$\mathrm{d}L_f\boldsymbol{h} = [\boldsymbol{O}_3 \ \boldsymbol{O}_3 \ \boldsymbol{O}_3 \ \boldsymbol{I}_3] \ . \tag{28}$$

The Lie derivatives along $\boldsymbol{g}_i$ are all equal to zero, i.e. $L_g\boldsymbol{h} = \boldsymbol{0}$. If we continue to compute the Lie derivatives and their differentials for upper order, we would find that it is not possible to construct an observation-space matrix $\mathcal{O}$ of rank greater than 6. That is a consequence of the vector fields $\boldsymbol{g}_i$ to be independent of the position $\boldsymbol{\xi}$.

Since the method employed here gives only sufficient conditions for observability, an alternative method such as the analysis of the undistinguishable dynamics trajectories (De La Guerra et al., 2015) can be useful to show that this case is not observable. Roughly speaking, the method consists on comparing two identical systems with the same inputs and outputs for all the time, while starting from different initial conditions. One can easily show that the undistinguishable trajectories are reduced to $\dot{\boldsymbol{\xi}}_{\mathrm{a}} = \dot{\boldsymbol{\xi}}_{\mathrm{b}}$. Since starting from two different initial conditions $\boldsymbol{\xi}_{\mathrm{a}0}$ and $\boldsymbol{\xi}_{\mathrm{b}0}$ satisfy the undistinguishable dynamics, it is concluded that this case is in fact non observable.

Remark 1. The same method can be applied for the case when only acceleration is measured, which leads to the well-known *drift* problem in mobile robots. □

3.3 Case 3

In this case, we only measure position i.e.$\boldsymbol{y} = \boldsymbol{\xi}$. Let us start again by taking the differential of this output

$$\mathrm{d}\boldsymbol{h} = [\boldsymbol{I}_3 \ \boldsymbol{O}_3 \ \boldsymbol{O}_3 \ \boldsymbol{O}_3] \ . \tag{29}$$

The Lie derivative along $\boldsymbol{f}$ is

$$L_f\boldsymbol{h} = \dot{\boldsymbol{\xi}} \, , \tag{30}$$

whose differential is

$$\mathrm{d}L_f\boldsymbol{h} = [\boldsymbol{O}_3 \ \boldsymbol{O}_3 \ \boldsymbol{I}_3 \ \boldsymbol{O}_3] \ , \tag{31}$$

and the Lie derivatives with respect to $\boldsymbol{g}_i, i = 1, \ldots, 4$ are all zero, i.e. $\mathrm{d}L_{g_i}\boldsymbol{h} = \boldsymbol{0}$.

In this case, since the vector field $\boldsymbol{g}_1$ does depend on $\boldsymbol{\eta}$ and both the differential $\mathrm{d}L_f\boldsymbol{h}$ and $\boldsymbol{g}_1$ have similar rows (7 to 9) with nonzero components, it is worth to keep following with the observation matrix construction. For this purpose, let us take the Lie derivative of the mentioned fields

$$L_{g_1 f}\boldsymbol{h} = \frac{\partial L_f\boldsymbol{h}}{\partial \boldsymbol{x}}\boldsymbol{g}_1 \doteq \boldsymbol{f}_{g_1 f}(\boldsymbol{\nu}) \, , \tag{32}$$

which is a function of $\boldsymbol{\nu}$ (in fact is the third column of $\boldsymbol{R}_{\mathrm{b}}$ divided by the mass m). Therefore, it is expected that its differential would have nonzero components in the 4th to 6th columns, i.e.

$$\mathrm{d}L_f\boldsymbol{h} = [\boldsymbol{O}_3 \ \mathrm{d}L_{g_1 f}\boldsymbol{h} \ \boldsymbol{O}_3 \ \boldsymbol{O}_3] \ . \tag{33}$$

Because from this point the computations become cumbersome, we resort on a symbolic computation software, namely, *Wolfram Mathematica* to carry out our computation of the observability matrix. After some explorations, the employed differentials, in addition to the above, to compute the observability matrix are

$$\mathcal{O} = \begin{bmatrix} \mathrm{d}\boldsymbol{h} \\ \mathrm{d}L_f \\ \mathrm{d}L_{fg_1 f}\boldsymbol{h} \\ \mathrm{d}L_{g_2 fg_1 f}\boldsymbol{h} \\ \mathrm{d}L_{g_3 fg_1 f}\boldsymbol{h} \\ \mathrm{d}L_{fg_2 fg_1 f}\boldsymbol{h} \, , \end{bmatrix} \tag{34}$$

where the remaining differentials, evaluated in the operation point of interest, i.e. around $\boldsymbol{\xi} = (x_0, y_0, z_0)$, $\dot{\boldsymbol{\xi}} = \boldsymbol{\eta} = \dot{\boldsymbol{\eta}} = \boldsymbol{0}$, are computed as

$$\mathrm{d}L_{fg_1 f}\boldsymbol{h} = \begin{bmatrix} \boldsymbol{O}_3 \ \boldsymbol{O}_3 \ \boldsymbol{O}_3 \ \begin{bmatrix} 0 & 1/m & 0 \\ -1/m & 0 & 0 \\ 0 & 0 & 0 \end{bmatrix} \end{bmatrix}$$

$$\mathrm{d}L_{g_2 fg_1 f}\boldsymbol{h} = \begin{bmatrix} \boldsymbol{O}_3 \ \begin{bmatrix} 0 & 0 & 1/(I_x m) \\ 0 & 0 & 0 \\ -1/(I_x m) & 0 & 0 \end{bmatrix} \ \boldsymbol{O}_3 \ \boldsymbol{O}_3 \end{bmatrix}$$

$$\mathrm{d}L_{g_3 fg_1 f}\boldsymbol{h} = \begin{bmatrix} \boldsymbol{O}_3 \ \begin{bmatrix} 0 & 0 & 0 \\ 0 & 0 & 1/(I_y m) \\ 0 & -1/(I_y m) & 0 \end{bmatrix} \ \boldsymbol{O}_3 \ \boldsymbol{O}_3 \end{bmatrix}$$

$$\mathrm{d}L_{fg_2 fg_1 f}\boldsymbol{h} = \begin{bmatrix} \boldsymbol{O}_3 \ \boldsymbol{O}_3 \ \boldsymbol{O}_3 \ \begin{bmatrix} 0 & 0 & 1/(I_x m) \\ 0 & 0 & 0 \\ -1/(I_x m) & 0 & 0 \end{bmatrix} \end{bmatrix} \, .$$

As a result, this analysis demonstrates that it is possible, at least theoretically, to reconstruct all the state vector $\boldsymbol{x}$ by measuring only the Cartesian positions and the control inputs.

3.4 Case 4

The last case is a particular scenario motivated from Case 3, where it was shown that one can reconstruct the whole state with ony relying on linear position measurements. However, the method do not tell us how to construct a suitable state-observer, which can be a very difficult task. Some observer constructive methods are based on the observability mapping (Besancon and Ticlea, 2007). Nevertheless, the observer design becomes more complicated as higher order Lie derivatives are included. For such reason, it would be convenient to reduce the order of the Lie derivatives employed to compute (34). This can be done if one notice that in such mapping, the most difficult columns to obtain with nonzero components are those related with the yaw angle.

Thus, if we consider the case in which this angle ψ is measured along with the linear position, i.e. $\boldsymbol{y} = [x \ y \ z \ \psi]^{\mathrm{T}}$, then one can obtain a full column-rank observability matrix by computing

 https://doi.org/10.58571/CNCA.AMCA.2025.041

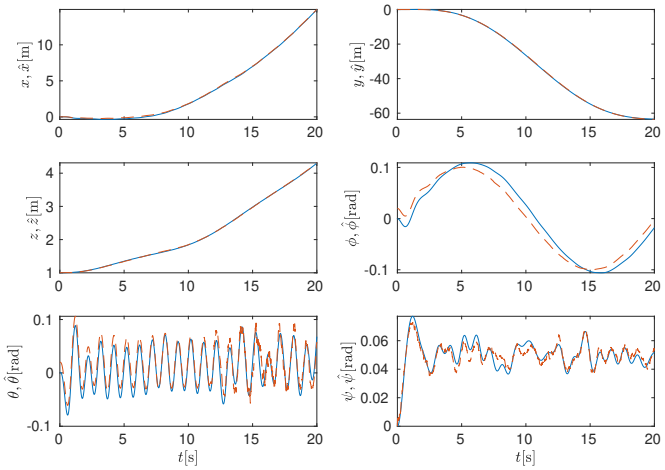

Fig. 2. Real (—) and estimated (- - -) positions and angles for Case 4.

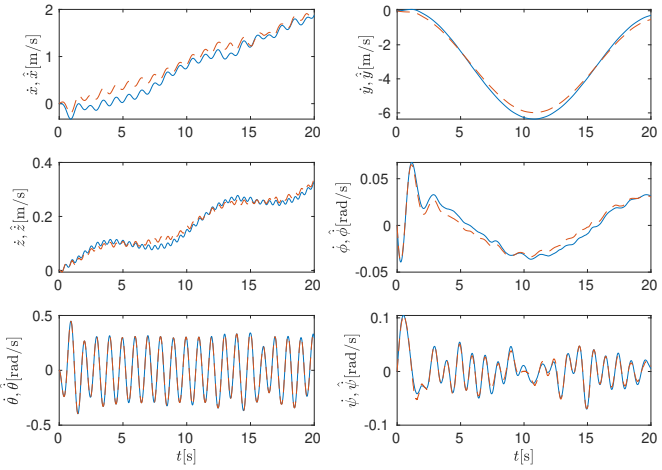

Fig. 3. Real (—) and estimated (- - -) time-derivatives for Case 4.

$$\mathcal{O} = \begin{bmatrix} \mathrm{d}\boldsymbol{h} \\ \mathrm{d}L_f \\ \mathrm{d}L_{g_1 f}\boldsymbol{h} \\ L_{fg_1 f}\boldsymbol{h} \end{bmatrix}, \tag{35}$$

which has the additional advantage of depending only on the vector field $\boldsymbol{g}_1$ associated with the input $u_1 = T$, i.e. the thrust of the quadrotor in body coordinates.

4. SIMULATION

A simulation study in Matlab/Simulink was carried out to validate the observability analysis above. The parameters of the quadrotor for the dynamics simulation were taken from Pham et al. (2019). An extended Kalman filter (EKF) was implemented for the Case 4 analyzed in Section 3.4. Since for this case, the system is not uniformly observable, the following inputs were considered:

$$\begin{aligned} u_1 =& m(mg_0 + 0.05 - 0.1\sin(4\pi t/T)) \\ u_2 =& -0.1(\hat{\phi} - 0.1\sin(0.1\pi t/T)) - 0.01\dot{\hat{\phi}} \\ u_3 =& -0.1(\hat{\theta} - 0.02 + 0.1\sin(2\pi t/T)) - 0.01\dot{\hat{\theta}} \\ u_4 =& -0.1(\hat{\psi} - 0.05) - 0.01\dot{\hat{\psi}}\,. \end{aligned}$$

A zero-mean Gaussian noise with covariance $cov = 0.01$ was added to all measured outputs. The observer states were initialized with different values for the non-measured states, whereas the real values were employed to initialize the measured ones. For the EKF implementation, there were considered $\boldsymbol{P}(t_0) = 0.1\boldsymbol{I}_12$, $\boldsymbol{Q} = 0.01\boldsymbol{I}_12$, $\boldsymbol{R} = 0.01\boldsymbol{I}_4$.

The time evolution of the measured and estimated pose variables are shown in Figure 2, whereas their time-derivatives are shown in Figure 3. In these figures, there can be seen that the estimated stated converge to the real ones, despite the noise.

5. DISCUSSION

The results of the cases analyzed in this paper are summarized in Table 1.

Table 1. Comparison of sensor configurations and observability.

Outputs	Observable	Input dependent	Inputs used
$\boldsymbol{\xi}, \boldsymbol{\eta}$	Yes	No	No
$\boldsymbol{\eta}$	No	–	–
$\boldsymbol{\xi}$	Yes	Yes	u_1, u_2, u_3
x, y, z, ψ	Yes	Yes	u_1

Although Case 1 is a trivial one, is the most employed in the control of quadcopters, since positions and roll-pitch-yaw angles are measured and velocities are commonly estimated by different techniques, ranging from numerical differentiation to nonlinear observers. This case is uniformly observable, therefore, it is not necessary to have active inputs for state estimation, which is a great advantage in the observer design.

In turn, Case 2, in which only the orientation variables are measured, i.e. the roll-pitch-yaw angles, resulted to be non-observable. This case is of importance in drone control since most UAVs have an inertial measurement unit (IMU), an accelerometer, and a magnetometer. This case would be equivalent to having just these sensors and no external ones such as global position system (GPS), motion tracking systems, or a camera. Although cameras have become less and less expensive and some algorithms such a SLAM have been evolving during the last years, the low latency of the signals acquired from these sensors is still a big drawback for implementing advanced controllers.

A remarkable result of this study is the one presented in Case 3, where only the Cartesian position of the drone center of mass is measured. Although the observability resulted to be non-uniform, i.e. it depends on the input, it is possible to construct a full-rank observability mapping,

 https://doi.org/10.58571/CNCA.AMCA.2025.041

which guarantees local observability around the point of interest (hoovering). This result is not intuitive and has some potential applications, e.g. for space robots, where a magnetometer might not work but a reliable on-ground station could estimate the UAV position.

Finally, we present Case 4, which is very similar to Case 3, but adding the measurement of the yaw angle. By adding this output, the dimension of the observability mapping is reduced and, although the observability still depends of the input, only the first input-related vector field is employed to construct it. These two advantages could be of paramount importance for designing a state observer and a control strategy. For this case, a simulation study of an Extended Kalman Filter was presented, which showed the feasibility of implementing an observer. It is worth to point out that the design of a good input is not a trivial task, since it must be persistently exciting Besançon (2007) for the observer to converge.

6. CONCLUSIONS

In this paper, we have presented a dynamic model, based on the Euler–Lagrange formulation, for quadrotor unmanned aerial vehicles. This model is employed as a starting point for analyzing the state observability of four possible configurations of measured variables. The results show that the system is uniformly observable when both linear and angular positions are measured, non-observable when only angular positions are measured, and non-uniformly observable when only linear positions are measured. In addition, we analyze the case in which the positions and the yaw rotation angle are measured, resulting again in a non-uniformly observable system, but more suitable for observer and controller designs.

As future work, it remains to design a methodology to find the conditions on the input to have observability and to design a close-loop controller based on the observer estimations. In particular, the last analyzed case is of interest since it presents the required conditions to apply a constructive methodology with less terms. Nevertheless, the observer design for the case of only linear position measurements will still be pursued.

REFERENCES

Artale, V., Milazzo, C., and Ricciardello, A. (2013). Mathematical modeling of hexacopter. *Applied mathematical sciences*, 7(97), 4805–4811.

Besançon, G. (2007). *Nonlinear observers and applications*, volume 363. Springer.

Besancon, G. and Ticlea, A. (2007). An immersion-based observer design for rank-observable nonlinear systems. *IEEE Transactions on Automatic Control*, 52(1), 83–88.

De La Guerra, A., Maya-Ortíz, P., and Espinosa-Pérez, G. (2015). Global observability analysis of the sr motor under sensorless operation. In *2015 54th IEEE Conference on Decision and Control (CDC)*, 1799–1804. IEEE.

Hermann, R. and Krener, A. (1977). Nonlinear controllability and observability. *IEEE Transactions on Automatic Control*, 22(5), 728–740. doi: 10.1109/TAC.1977.1101601.

Isidori, A. (1985). *Nonlinear control systems: an introduction*. Springer.

Luukkonen, T. (2011). Modelling and control of quadcopter. *Independent research project in applied mathematics, Espoo*, 22(22), 1–24.

Olivares-Figueroa, J.D., Cruz-Vega, I., Gutierrez-Giles, A., and Martinez-Carranza, J. (2024). Spherical aerial manipulator robot for exploration in complex forest environments. In *Proceedings of the 2024 International Micro-Air Vehicles Conference, Bristol, United Kingdom*.

Parlange, R., Martinez-Carranza, J., Sucar, L., Ren, B., and Watkins, S. (2018). Vision-based autonomous navigation for wind turbine inspection using an unmanned aerial vehicle. In *Proceedings of the 10th International Micro-Air Vehicles Conference, Melbourne, Australia*, 22–23.

Pham, T.H., Ichalal, D., and Mammar, S. (2019). Lpv and nonlinear-based control of an autonomous quadcopter under variations of mass and moment of inertia. *IFAC-PapersOnLine*, 52(28), 176–183.

Quero, C.O. and Martinez-Carranza, J. (2025). Unmanned aerial systems in search and rescue: A global perspective on current challenges and future applications. *International Journal of Disaster Risk Reduction*, 105199.

Ramachandran, A. and Sangaiah, A.K. (2021). A review on object detection in unmanned aerial vehicle surveillance. *International Journal of Cognitive Computing in Engineering*.

Siciliano, B., Sciavicco, L., Villani, L., and Oriolo, G. (2010). *Robotics: Modelling, Planning and Control*. Advanced Textbooks in Control and Signal Processing. Springer London. URL `https://books.google.com/books?id=jPCAFmE-logC`.

Sonugür, G. (2023). A review of quadrotor uav: Control and slam methodologies ranging from conventional to innovative approaches. *Robotics and Autonomous Systems*, 161, 104342.

Spong, M.W., Hutchinson, S., Vidyasagar, M., et al. (2006). *Robot modeling and control*, volume 3. Wiley New York.

Vazquez-Meza, V.E. and Martinez-Carranza, J. (2024). Landing zone detection for mavs using depth images and vision transformers. In *Proceedings of the 2024 International Micro-Air Vehicles Conference, Bristol, United Kingdom*.

Wang, X., He, N., Hong, C., Wang, Q., and Chen, M. (2023). Improved yolox-x based uav aerial photography object detection algorithm. *Image and Vision Computing*, 135, 104697.

 https://doi.org/10.58571/CNCA.AMCA.2025.041